AIAA SciTech Forum
11–15 & 19–21 January 2021, VIRTUAL EVENT
AIAA Scitech 2021 Forum

10.2514/6.2021-0853

Effect of wall cooling or heating on streaks in high-speed boundary layers

Omar Es Sahli *[1], Adrian Sescu†[1], Mohammed Afsar‡[2], Yuji Hattori§[3], and Makoto Hirota¶[3]

[1]Department of Aerospace Engineering, Mississippi State University, MS 39762
[2]Department of Mechanical & Aerospace Engineering, Strathclyde University, 75 Montrose St. Glasgow, G1 1XJ, UK
[3]Institute of Fluid Science, Tohoku University, 2 Chome-1-1 Katahira, Aoba Ward, Sendai, 980-8577, Japan

High-amplitude upstream disturbances and wall surface roughness elements trigger streamwise/Görtler vortices and the associated streaks in boundary layers over flat or concave surfaces. Following the transient growth phase, the fully-developed vortices become sensitive to inviscid secondary instabilities, which ultimately result in a premature transition to turbulence. Our work aims at investigating the effect of cooling/heating on the initiation and development of such streaks in an attempt to gain a better understanding of the conditions and governing mechanisms leading to secondary instabilities in high-speed compressible boundary layers. We conduct a parametric study via a robust and efficient numerical solution to the non-linear compressible boundary region equations (NCBRE) to identify the impact of varying the wall temperature on the development of streaks in supersonic and hypersonic boundary layer flows.

I. Introduction

Motivated by numerous engineering applications such as high-speed flow in engine intakes, flows over the concave surface of turbomachinery blades, or flows over the walls of supersonic nozzles, to mention few, researchers have been studying Görtler vortices in boundary layers for quite a while. For instance, Kobayashi and Kohama[21] incorporated parallel flow theory to study these vortices while the non-parallel effects were studied by El-Hady and Verma,[5] Hall and Fu,[17] and Hall and Malik.[18] Spall and Malik[42] further improved the parallel eigenvalue framework by adding initial conditions to the partial differential equations assuming zero amplitude perturbations in the external boundary layer. Nevertheless, in the literature, there are fewer experiments involving Görtler vortices developing in compressible boundary layers compared to the large number of experiments performed in the incompressible regime. Therefore, topics pertaining to the compressible regime such as streak development in flows over concave surfaces or bypass transition remain largely unexplored.

Streamwise oriented vortices in compressible boundary layer flows coexist with elongated streamwise velocity structures (streaks) characterized by juxtaposed regions of accelerated (high-speed) and decelerated (low-speed) fluid particles (e.g., Kendall,[20] Matsubara & Alfredsson,[30] or Landahl[22]). The formation of these streaks in pre-transitional boundary layer flows takes place either when the amplitude of the freestream disturbances exceeds a certain threshold (e.g., Kendall,[20] Westin et al.,[46] Matsubara & Alfredsson,[30] Leib et al.,[23] Zaki & Durbin,[53] Goldstein & Sescu,[11] or Ricco et al.[34]), or when the height of the roughness elements of the surface passes a given critical value (e.g., Choudhari & Fischer,[2] White,[47] White et al.,[48]

*Research Assistant, Department of Aerospace Engineering, Mississippi State University, MS 39762; member AIAA.
†Associate Professor, Department of Aerospace Engineering, Mississippi State University; Associate Fellow AIAA.
‡Chancellor Fellow, Department of Mechanical & Aerospace Engineering; AIAA member.
§Professor, Institute of Fluid Science, Tohoku University.
¶Assistant Professor, Institute of Fluid Science, Tohoku University.

Goldstein et al.,[8–10] or Wu & Choudhari[49]). These streamwise vortices also occur in boundary layer flows over concave surfaces due to the imbalance between the wall radial pressure gradients and centrifugal forces (e.g., Gortler,[12] Hall,[14–16] Swearingen & Blackwelder,[43] Malik & Hussaini,[28] Saric,[37] Li & Malik,[24] Boiko et al.,[1] Wu et al.,[50] or Sescu et al.,[39,40] Ren & Fu,[32] Dempsey et al.,[3] Xu et al.[51]). Walls with high curvature result in a more rapid vortex formation which significantly alters the mean flow, thus, forcing the breakdown of laminar flow into turbulence.

Studies aiming to establish the correlation between the transition Reynolds number and freestream turbulence (FST) level have shown that the FST level (Dryden,[4] Schneider[41]) and surface roughness (e.g. Pate[31]) significantly shift the position where transition takes place. Yet, only few investigations cover the detailed physics underlying such correlation. The work of Kendall[19] provide much information about supersonic boundary-layer transition under the influence of a high level of FST. A salient feature is that fluctuations over a wide frequency range undergo substantial growth within the boundary layer. Sufficiently downstream, a spectral peak emerges corresponding to the Mack-I mode in the low-Mach-number supersonic range (M < 4.5) (Mack[27]). For higher Mach numbers, a secondary, less pronounced peak representing the Mack-II instability is observed. These results indicate that some type of receptivity mechanism operates to generate instability waves in a nominally flat plate.

Ricco & Wu[34] extended the incompressible analysis by Leib et al.[23] to the compressible regime and explained the formation and growth of thermal streaks, which are thought to play a significant role in the secondary instability process. Ricco, Tran & Ye[36] and Ricco, Shah & Hicks,[35] respectively, further studied the influence of wall heat transfer and wall suction on thermal streaks.

In this paper, we focus our investigation on streamwise vortices and the associated streaks evolving in high-speed boundary layers using the non-linear compressible boundary region equations (NCBRE) formalism which represent a high Reynolds number asymptotic form of the Navier-Stokes equations. The NCBRE are derived under the assumption that the streamwise wavenumber of the disturbances is much smaller than the $O(1)$ wavenumber associated with the spanwise direction. This set of equations is parabolic in the streamwise direction allowing for a straightforward marching procedure to be applied in this direction. Görtler vortices are excited via a steady transpiration velocity imposed at the wall in proximity to the upstream boundary. We conduct a parametric analysis to identify the impacts of varying the wall temperature on the development of streaks in the boundary layer at supersonic and hypersonic freestream Mach number conditions.

The rest of the paper is organized as follow: In section II, we introduce the mathematical model and discuss the scalings of various independent and dependent variables, the appropriate initial and boundary conditions, as well as the numerical algorithm. In section III, we report and discuss results for various wall-temperatures at supersonic and hypersonic freestream Mach number conditions. We reserve section IV for concluding remarks.

II. Problem formulation and numerical algorithm

We consider a compressible flow of uniform velocity V_∞^* and temperature T_∞^* past a flat or curved surface. The air is treated as a perfect gas such that the sound speed in the free-stream $c_\infty^* = \sqrt{\gamma R T_\infty^*}$, where $\gamma = 1.4$ is the ratio of the specific heats, and $R = 287.05 Nm/(kgK)$ is the universal gas constant; Mach number is assumed to be of order one. The flow is divided into four regions as in Leib et al.,[23] Ricco & Wu[34] or Marensi et al.:[29]

- Region I is in proximity to the the leading edge, outside of the boundary layer, where the flow is assumed inviscid and the disturbances are treated as small perturbations of the base flow.
- Region II is the boundary layer in the vicinity of the leading edge, with the thickness much smaller than the spanwise separation associated with the freestream disturbances. In this region, the disturbances are governed by the linearized boundary region equations, and the diffusion in the spanwise direction is in the same order of magnitude as that in the wall-normal direction.
- Region III is the viscous region that follows in the downstream of region II; here, the boundary layer thickness is in the same order of magnitude as the spanwise separation. The flow is governed by the boundary-region equations, which are obtained from the full Navier-Stokes equations by neglecting the streamwise pressure-gradient and the streamwise viscous diffusion.

- Region IV is above region III, and the flow is assumed again inviscid since the viscous effects are negligible. In this region, the flow is influenced at leading order by the displacement effect due to the increased thickness of the viscous layer underneath.

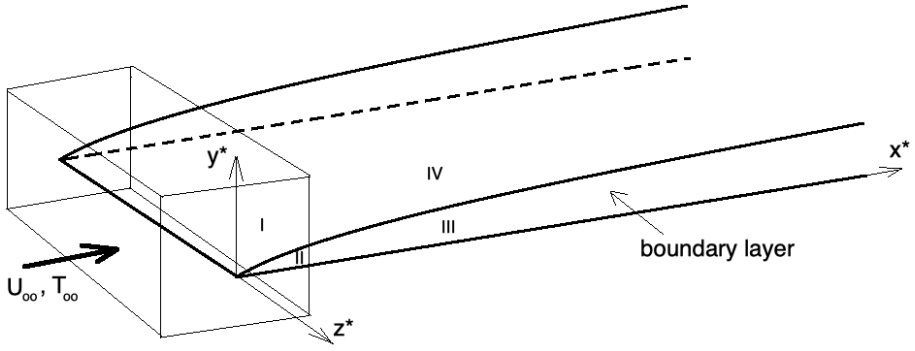

Figure 1. The flow domains illustrating the asymptotic structure.

The focus in this paper is on region III, where the streamwise wavenumber of disturbances are expected to be small and the flow is governed by the compressible boundary region equations.

A. Scalings

All dimensional spatial coordinates (x^*, y^*, z^*) are normalized by the spanwise separation λ^* of the disturbances, while the dependent variables by their respective freestream values. The pressure field is normalized by the dynamic pressure as follows

$$\bar{t} = \frac{t^*}{\lambda^*/V_\infty^*}; \quad \bar{x} = \frac{x^*}{\lambda^*}; \quad \bar{y} = \frac{y^*}{\lambda^*}; \quad \bar{z} = \frac{z^*}{\lambda^*} \tag{1}$$

$$\bar{u} = \frac{u^*}{V_\infty^*}; \quad \bar{v} = \frac{v^*}{V_\infty^*}; \quad \bar{w} = \frac{w^*}{V_\infty^*}; \quad \bar{\rho} = \frac{\rho^*}{\rho_\infty^*} \tag{2}$$

$$\bar{p} = \frac{p^* - p_\infty^*}{\rho_\infty^* V_\infty^{*2}}; \quad \bar{T} = \frac{T^*}{T_\infty^*}; \quad \bar{\mu} = \frac{\mu^*}{\mu_\infty^*}; \quad \bar{k} = \frac{k^*}{k_\infty^*} \tag{3}$$

where λ^* is the spanwise wavelength of the disturbances, (u^*, v^*, w^*) are the velocity components, ρ^* the density, p^* is pressure, T^* temperature, μ^* dynamic viscosity, k^* thermal conductivity and all quantities with ∞ at the subscript represent conditions at infinity.

Reynolds number based on the spanwise separation, Mach number and Prandtl number are defined as

$$R_\lambda = \frac{\rho_\infty^* V_\infty^* \lambda^*}{\mu_\infty^*}, \qquad Ma = \frac{V_\infty^*}{a_\infty^*}, \qquad Pr = \frac{\mu_\infty^* C_p}{k_\infty^*} \tag{4}$$

where μ_∞^*, a_∞^* and k_∞^* are freestream dynamic viscosity, speed of sound and thermal conductivity, respectively, and C_p is the specific heat at constant pressure. For boundary layer flows over curved surfaces, we define the global Görtler number as

$$G_\lambda = \frac{R_\lambda^2 \lambda^*}{r^*} \tag{5}$$

where r^* is the radius of the curvature.

B. Compressible boundary-region equations

For a full compressible flow, the primitive form of the Navier-Stokes equations in non-dimensional variables are considered here in the form

$$\frac{D\bar{\rho}}{Dt} + \rho\nabla\cdot\bar{\mathbf{u}} = 0 \tag{6}$$

$$\bar{\rho}\frac{D\bar{\mathbf{u}}}{D\bar{t}} = -\nabla\bar{p} + \frac{1}{Re_\lambda}\frac{\partial}{\partial\bar{x}_j}\left[\bar{\mu}\left(\frac{\partial\bar{u}_i}{\partial\bar{x}_j} + \frac{\partial\bar{u}_j}{\partial\bar{x}_i}\right) - \frac{2}{3}\bar{\mu}\delta_{ij}\nabla\cdot\bar{\mathbf{u}}\right] \tag{7}$$

$$\bar{\rho}\frac{D\bar{T}}{D\bar{t}} = \frac{1}{PrRe_\lambda}\nabla\cdot(\bar{k}\nabla\bar{T}) - (\gamma-1)M_\infty^2\left[p\nabla\cdot\bar{\mathbf{u}} - \frac{2}{3}\bar{\mu}(\nabla\cdot\bar{\mathbf{u}})^2\right] + (\gamma-1)M_\infty^2\frac{\bar{\mu}}{Re_\lambda}\Psi, \tag{8}$$

where

$$\Psi = 2\left(\frac{\partial\bar{u}}{\partial\bar{x}}\right)^2 + 2\left(\frac{\partial\bar{v}}{\partial\bar{y}}\right)^2 + 2\left(\frac{\partial\bar{w}}{\partial\bar{z}}\right)^2 + \left(\frac{\partial\bar{u}}{\partial\bar{y}} + \frac{\partial\bar{v}}{\partial\bar{x}}\right)^2 + \left(\frac{\partial\bar{w}}{\partial\bar{x}} + \frac{\partial\bar{u}}{\partial\bar{z}}\right)^2 + \left(\frac{\partial\bar{v}}{\partial\bar{z}} + \frac{\partial\bar{w}}{\partial\bar{y}}\right)^2 \tag{9}$$

is the dissipation function, and $D/D\bar{t} = \partial/\partial\bar{t} + \bar{u}\partial/\partial\bar{x} + \bar{v}\partial/\partial\bar{y} + \bar{w}\partial/\partial\bar{z}$ is the substantial derivative. The pressure p, the temperature T and the density of the fluid are combined in the equation of state in non-dimensional form, $\bar{p} = \bar{\rho}\bar{T}/\gamma M_\infty^2$, assuming that non-chemically-reacting flows are considered. Other notations include the dynamic viscosity μ, Reynolds number $Re = \rho_\infty V_\infty^*\lambda^*/\mu$ based on a characteristic velocity V_∞^*, and the spanwise separation λ^*, and the free-stream Mach number $M_\infty = V_\infty^*/a_\infty^*$. The dynamic viscosity and thermal conductivity k is linked to the temperature using the power law in dimensionless form,

$$\mu = T^b; \qquad k = \frac{C_p\mu}{Pr} \tag{10}$$

where $b = 0.76$, $C_p = \gamma R/(\gamma-1)$, $\gamma = 1.4$, and $Pr = 0.72$ for air.

Region III is where $x/R_\lambda = O(1)$, which implies that the streamwise ellipticity is weak and negligible (see Ricco & Wu,[34] Ricco,[33] or Marensi et al.[29]). The compressible boundary region equations can be derived from the full compressible Navier-Stokes equations. Based in the above assumption, the streamwise distance can be scaled as $x = \bar{x}/R_\lambda$ while the other two are the same $y = \bar{y}$, $z = \bar{z}$, and the time as $t = \bar{t}/R_\lambda$. Also, the crossflow components of velocity are expected to be small compared to the streamwise component, and variations of pressure are expected to be small. This suggests the asymptotic expansions with $1/R_\lambda$ as the small parameters:

$$\bar{u}(x,y,z) = u(x,y,z) + ...; \quad \bar{v}(x,y,z) = R_\lambda^{-1}v(x,y,z) + ...; \quad \bar{w}(x,y,z) = R_\lambda^{-1}w(x,y,z) + ...; \tag{11}$$

$$\bar{\rho}(x,y,z) = \rho(x,y,z) + ...; \quad \bar{p}(x,y,z) = R_\lambda^{-2}p(x,y,z) + ...; \bar{T}(x,y,z) = T(x,y,z) + ... \tag{12}$$

Inserting (23) into the full Navier-Stokes equations, and performing on order-of-magnitude analysis, the nonlinear compressible boundary region equations are obtained in the form

$$\begin{aligned}
&\frac{D\rho}{Dt} + \rho\nabla\cdot\vec{V} = 0\\
&\rho\frac{Du}{Dt} = \nabla_c\cdot(\mu\nabla_c u)\\
&\rho\frac{Dv}{Dt} = -\frac{\partial p}{\partial y} + \frac{\partial}{\partial y}\left[\frac{2}{3}\mu\left(3\frac{\partial v}{\partial y} - \nabla\cdot\vec{V}\right)\right] + \frac{\partial}{\partial x}\left(\mu\frac{\partial u}{\partial y}\right) + \frac{\partial}{\partial z}\left[\mu\left(\frac{\partial v}{\partial z} + \frac{\partial w}{\partial y}\right)\right] - G_\lambda u^2\\
&\rho\frac{Dw}{Dt} = -\frac{\partial p}{\partial z} + \frac{\partial}{\partial z}\left[\frac{2}{3}\mu\left(3\frac{\partial w}{\partial z} - \nabla\cdot\vec{V}\right)\right] + \frac{\partial}{\partial x}\left(\mu\frac{\partial u}{\partial z}\right) + \frac{\partial}{\partial y}\left[\mu\left(\frac{\partial v}{\partial z} + \frac{\partial w}{\partial y}\right)\right]\\
&\rho\frac{DT}{Dt} = \frac{1}{Pr}\nabla_c\cdot(k\nabla_c T) + (\gamma-1)M_\infty^2\mu\left[\left(\frac{\partial u}{\partial y}\right)^2 + \left(\frac{\partial u}{\partial z}\right)^2\right]
\end{aligned} \tag{13}$$

where ∇_c is the crossflow gradient operator:

$$\nabla_c = \frac{\partial}{\partial y}\vec{j} + \frac{\partial}{\partial z}\vec{k} \tag{14}$$

and $G_\lambda u^2$ is the term that accounts for the curvature.

This set of equations is parabolic in the streamwise direction and elliptic in the spanwise direction. Appropriate initial/upstream and boundary conditions are necessary to close the problem. One could use the same conditions as those used by Ricco & Wu[34] (see also Ricco[33]). However, our method uses a simpler alternative to excite the boundary layer using a small amplitude transpiration velocity (v_w) at the wall, in the form:

$$v_w = A \sin\left[\pi \frac{(x - x_s)}{(x_e - x_s)}\right]^2 \cos\left(\pi \frac{z}{\lambda}\right) \tag{15}$$

where A is the amplitude, x_s and x_e the start and end of the blowing and suction, and λ is the $O(1)$ spanwise separation.

The nonlinear compressible boundary equations were numerically solved using the algorithm of Es-Sahli et al.,[6] which proves robust and efficient as it provides results in a very short time compared to other mathematical models such as the parabolized stability equations (PSE) or direct numerical simulations (DNS).

The mean inflow condition is generated from the similarity solution, which is obtained by means of the Dorodnitsyn-Howarth coordinate transformation

$$\bar{Y}(x, y) = \int_0^y \rho(x, \tilde{y}) d\tilde{y} \tag{16}$$

A similarity variable is defined as

$$\eta = \bar{Y}\left(\frac{Re_x}{2x}\right)^{1/2}, \tag{17}$$

where Re_x is the Reynolds number based on the distance from the leading edge, and the base velocity and temperature can be expressed as

$$U = F'(\eta), \quad V = (2xRe_x)^{-1/2}(\eta_c T F' - TF), \quad T = T(\eta) \tag{18}$$

where prime represents differentiation with respect to η, and $\eta_c = 1/T \int_0^\eta T(\tilde{\eta}) d\tilde{\eta}$. F and T satisfy the following coupled equations

$$\begin{aligned} &\left(\frac{\mu}{T} F''\right)' + FF'' = 0, \\ &\frac{1}{Pr}\left(\frac{\mu}{T} T'\right)' + FT' + (\gamma - 1) M^2 \frac{\mu}{T} F''^2 = 0, \end{aligned} \tag{19}$$

satisfying the boundary conditions

$$F(0) = F'(0) = 0, \quad T'(0) = 0, \quad F' \to 1, \quad T \to 1 \to as \to \eta \to \infty \tag{20}$$

The dependence of the viscosity on the temperature is assumed to be described by the power law,

$$\mu = T^b, \quad b = 0.76 \tag{21}$$

Equations (19) were solved by a shooting method for both adiabatic and isothermal conditions. Figure 2 shows this solution for Mach number equal to 3, and for both isothermal and adiabatic wall conditions.

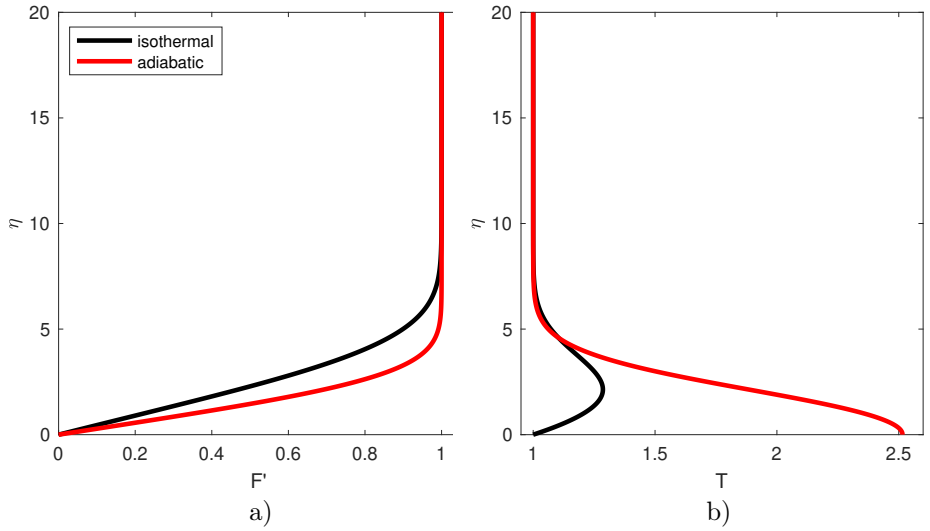

Figure 2. Base flow solution given by equation 20.

III. Results and discussion

We investigate the effect of heating or cooling on the development of Görtler vortices in high-speed boundary layers. The cooling or heating is imposed by varying the wall-temperature between 100 and 1500 Kelvin (K). Moreover, to study the effect of the Mach number, we consider cases of different Mach numbers ranging from supersonic, $M = 2$, to hypersonic conditions, $M = 6$ (note that since there are no obstructions in the flow, shock waves are not generated; see, for example, Li et al.[25] or Ren & Fu[32]). We consider cooling and heating to be wall-temperatures respectively smaller or higher than the adiabatic wall-temperature. We calculate the similarity solution forced at the upstream boundary using the Reynolds number based on the distance from the leading edge, which is maintained constant for a given Mach number.

For all cases considered in the parametric study, the concave surface has a radius of curvature of 2 m. We use a small disturbance applied to the vertical velocity imposed at the wall, with an amplitude of 0.2% of the freestream velocity, to excite the Görtlet vortices in the boundary layer as given by equation (15). Figure 3 is a schematic sketch of the flow domain, with region III highlighted in blue. The left hand side of figure 3 represents the upstream boundary of the domain where we impose the similarity type velocity and temperature profiles for a compressible boundary layer. Thus, the boundary layer develops from left to right in the streamwise parabolic direction. At the wall, we impose the no-slip boundary condition for the velocity vector components (u, v, w) and either an isothermal or adiabatic boundary condition for the temperature field. We impose vanishing gradients at the top boundary and a symmetry condition along the spanwise direction since we only simulate one streamwise vortex (corresponding to half of the mushroom shape), belonging to the pair of counter-rotating vortices.

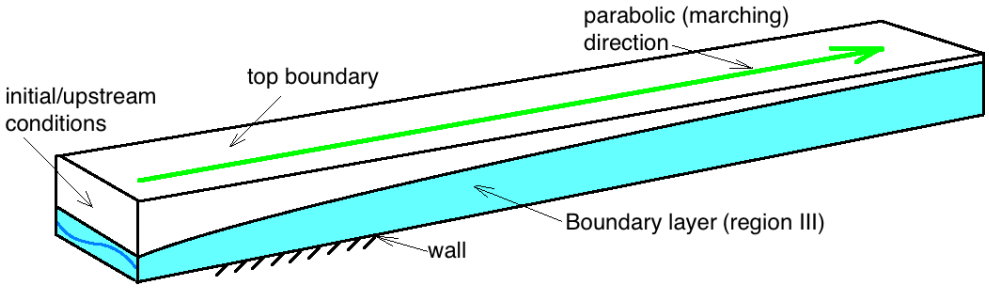

Figure 3. Flow domain.

We conduct a parametric study in which we examine the effect of varying the Mach number and wall-temperature on the development of secondary instabilities. Figures 4 and 5 display contour plots of temperature in consecutive cross-flow planes for different wall-temperatures at $M = 2$ and $M = 5$, respectively. The contours illustrate the streamwise development of the temperature field of the Görtler vortices characterized by the mushroom-shape structures. Although, from a practical standpoint, it makes more sense to only consider cooling for high Mach numbers, especially in the hypersonic regime since the flow temperature can become higher than the applied wall-temperatures considered in this study, we sought to include all results for consistency. In the contour plots, blue and green correspond to the low-temperature streaks whereas red regions are associated with high-temperature streaks. Es-Sahli et al.[6] reported that the high- and low-temperature streaks are respectively associated with low- and high-velocity streaks. In figure 4 ($M = 2$), contour plots in (a), (b), and (c) correspond to cooling while (d), (e), and (f) to heating, see figure 7a, whereas in figure 5 (M=5), only (f) correspond to heating and the rest of the contour plots correspond to cooling, see figure 7d.

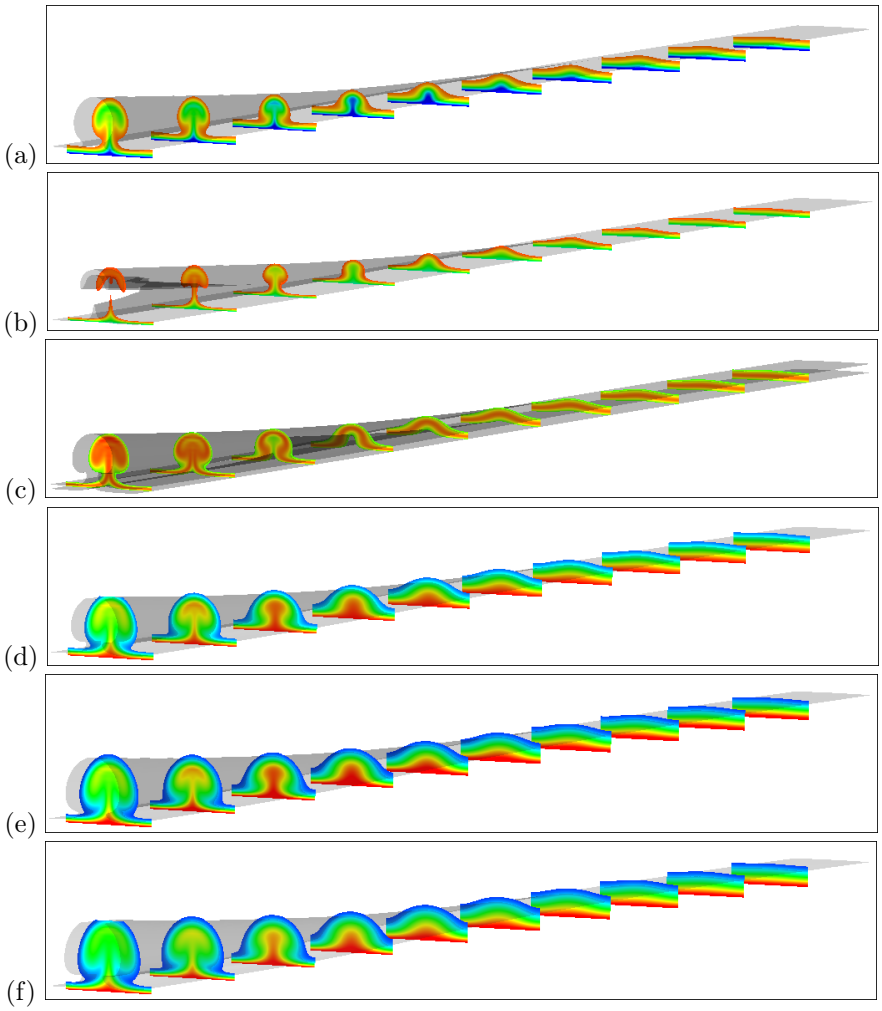

Figure 4. Contour plots of temperature in crossflow planes for different wall-temperatures: a) 100 K, b) 200 K, c) 300 K, d) 600 K, e) 900 K, and f) 1500 K for a mach number M=2.0

For the supersonic Mach number case, figure 4, the size (height and width) of the mushroom-shape structures corresponding to the heating cases are significantly larger than the ones corresponding to the cooling cases. For the heating condition cases, the size of the mushroom-shapes is directly proportional to the wall temperature due to the growth of thermals inside the structures. The thermals are created by the upward flow forced by the juxtaposed counter-rotating vortices. They grow as the wall-temperature is increased (with respect to the adiabatic wall-temperature). As the wall-temperature is decreased, however,

these thermals reduce in size resulting in smaller structures and consequently a smaller boundary layer thickness (although the structures corresponding to the 200 K wall-temperature appear narrower than the 100 K cases, which is an interesting observation suggesting further examination). On the other hand, contour plots of the hypersonic Mach number case, figure 5, show a steady trend of the mushroom-shape structures gradually increasing in size as the wall-temperature is increased with the heating case boundary layer thickness being the largest.

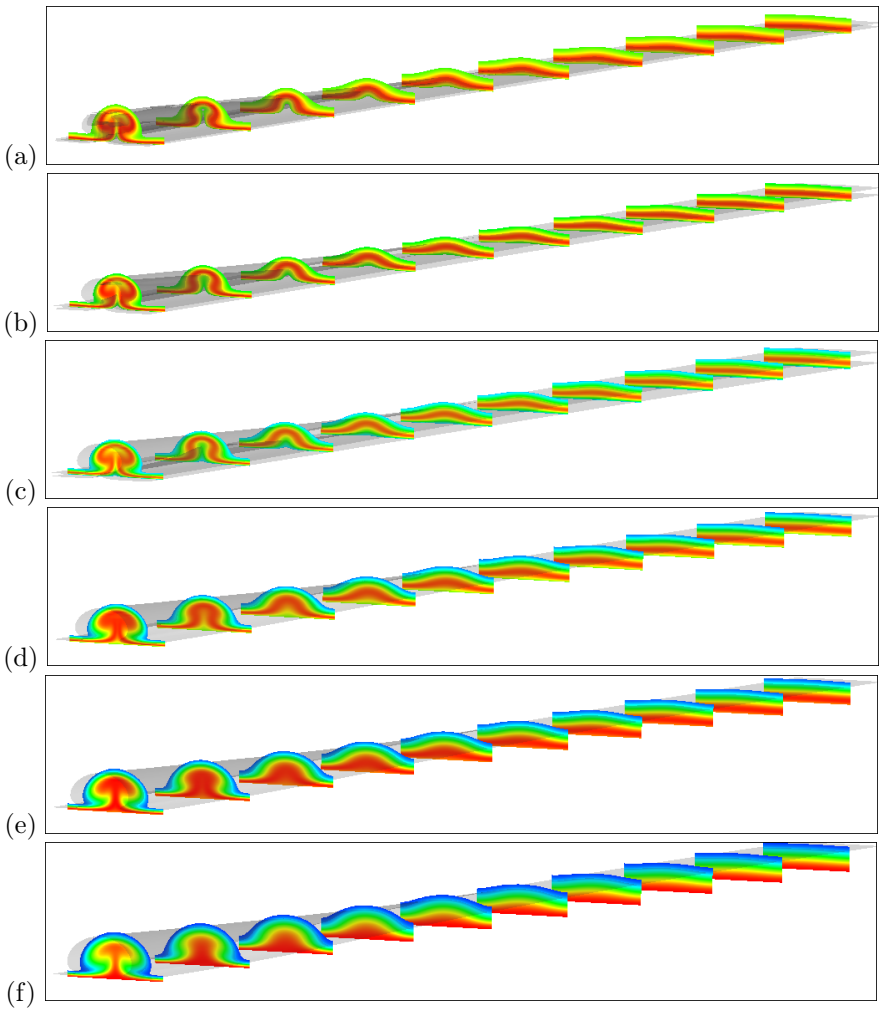

Figure 5. Contour plots of temperature in crossflow planes for different wall-temperatures: a) 100 K, b) 200 K, c) 300 K, d) 600 K, e) 900 K, and f) 1500 K for a mach number M=5.0

In figures 6 and 7, we plot selected profiles of velocity and temperature at different Mach numbers in the normal direction at the streamwise and spanwise coordinates corresponding, respectively, to the maximum vortex energy (see figure 8) and the center of the domain. For all Mach numbers, the velocity profiles indicate a reduction in the boundary layer thickness corresponding to the cooling cases ($<$ adiabatic wall-temperature) and an increase in the boundary layer thickness for cases corresponding to the heating cases ($>$ adiabatic wall-temperature). This quantitative result agrees with and supports the contour plots qualitative observations. However, the profiles start coalescing and the difference (increase/decrease) between the various wall-temperature cases becomes less significant as the Mach number is increased.

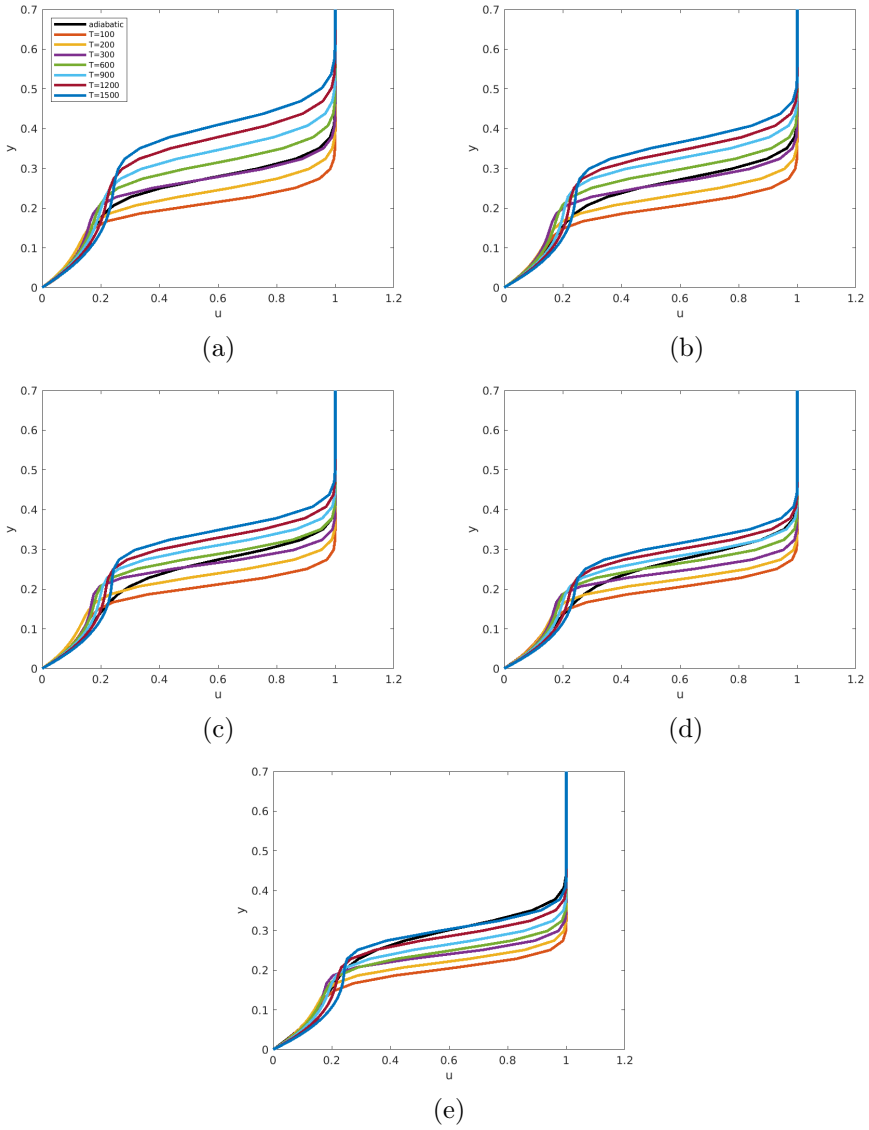

Figure 6. Streamwise velocity profiles for wall-temperatures; 100 K, 200 K, 300 K, 600 K, 900 K, 1200 K, and 1500 K at different freestream Mach number conditions: a) $M = 2.0$**, b)** $M = 3.0$**, c)** $M = 4.0$**, d)** $M = 5.0$**, e)** $M = 6.0$

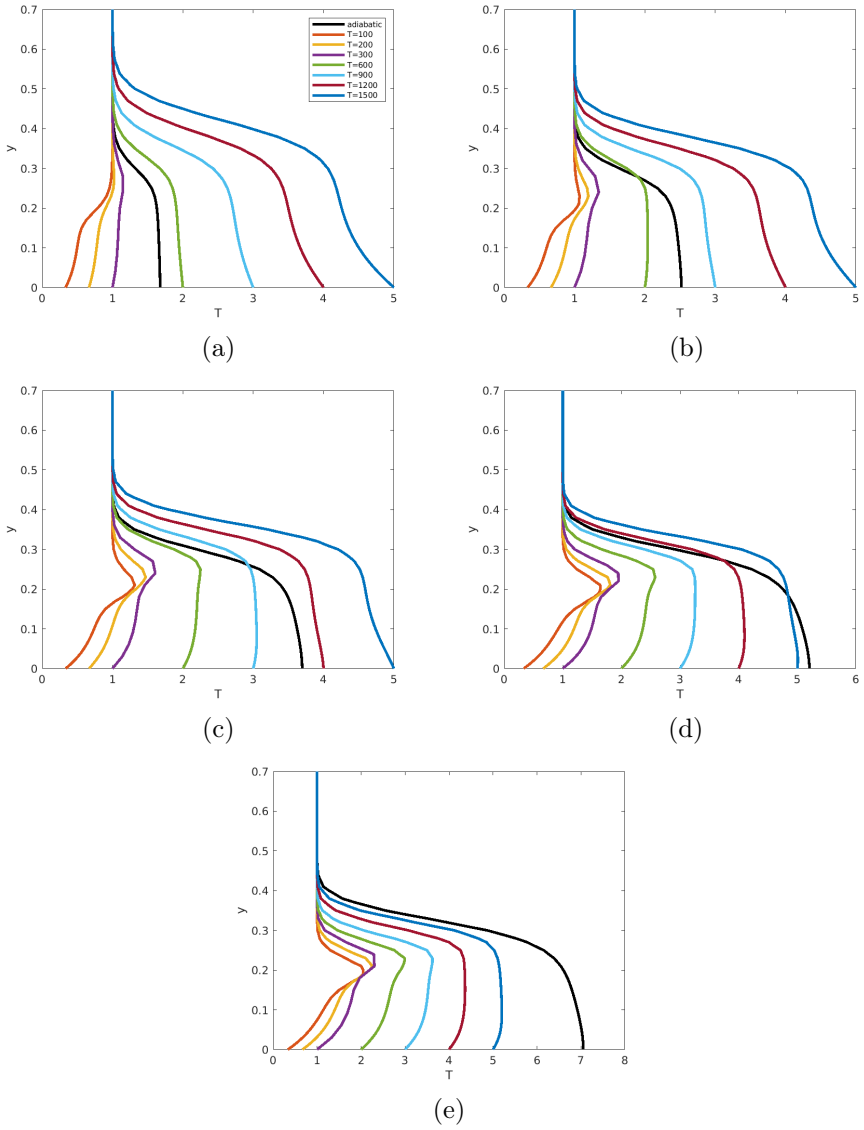

Figure 7. Temperature profiles for wall-temperatures; 100 K, 200 K, 300 K, 600 K, 900 K, 1200 K, and 1500 K at different freestream Mach number conditions: a) $M = 2.0$, b) $M = 3.0$, c) $M = 4.0$, d) $M = 5.0$, e) $M = 6.0$

We quantify the vortex energy as

$$E(x) = \int_{z_1}^{z_2} \int_{0}^{\infty} \left[|u(x,y,z) - u_m(x,y)|^2 + |v(x,y,z) - v_m(x,y)|^2 + |w(x,y,z) - w_m(x,y)|^2 \right] dzdy, \tag{22}$$

where $u_m(x,y)$, $v_m(x,y)$, and $w_m(x,y)$ are the spanwise mean components of velocity, and z_1 and z_2 are the coordinates of the spanwise domain boundaries.

In figures 8 and 9, we plot the vortex energy from equation (13) and the energy growth ($1/x \times dE/dx$) against the streamwise coordinate, x. We notice the same trend here as the cooling condition depicts less vortex energy and energy growth levels compared to heating. As for the adiabatic case, the vortex energy as well as the energy growth level increase significantly as the streamwise Mach number is increased. We also notice a delay in both the vortex energy and energy growth associated with the adiabatic case for the supersonic Mach number cases (a), (b), and (c) as opposed to the hypersonic cases (d) and (e).

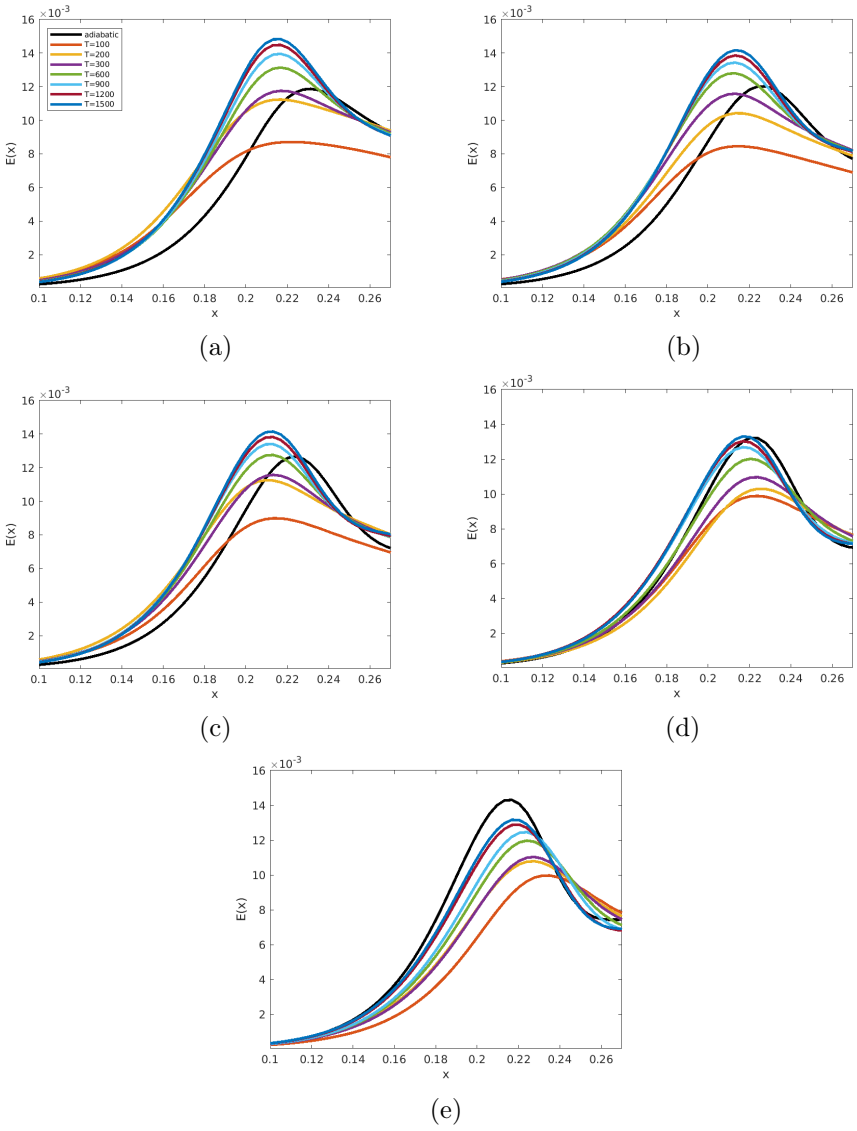

Figure 8. Vortex energy profiles for wall-temperatures; 100 K, 200 K, 300 K, 600 K, 900 K, 1200 K, and 1500 K at different freestream Mach number conditions: a) $M = 2.0$**, b)** $M = 3.0$**, c)** $M = 4.0$**, d)** $M = 5.0$**, e)** $M = 6.0$

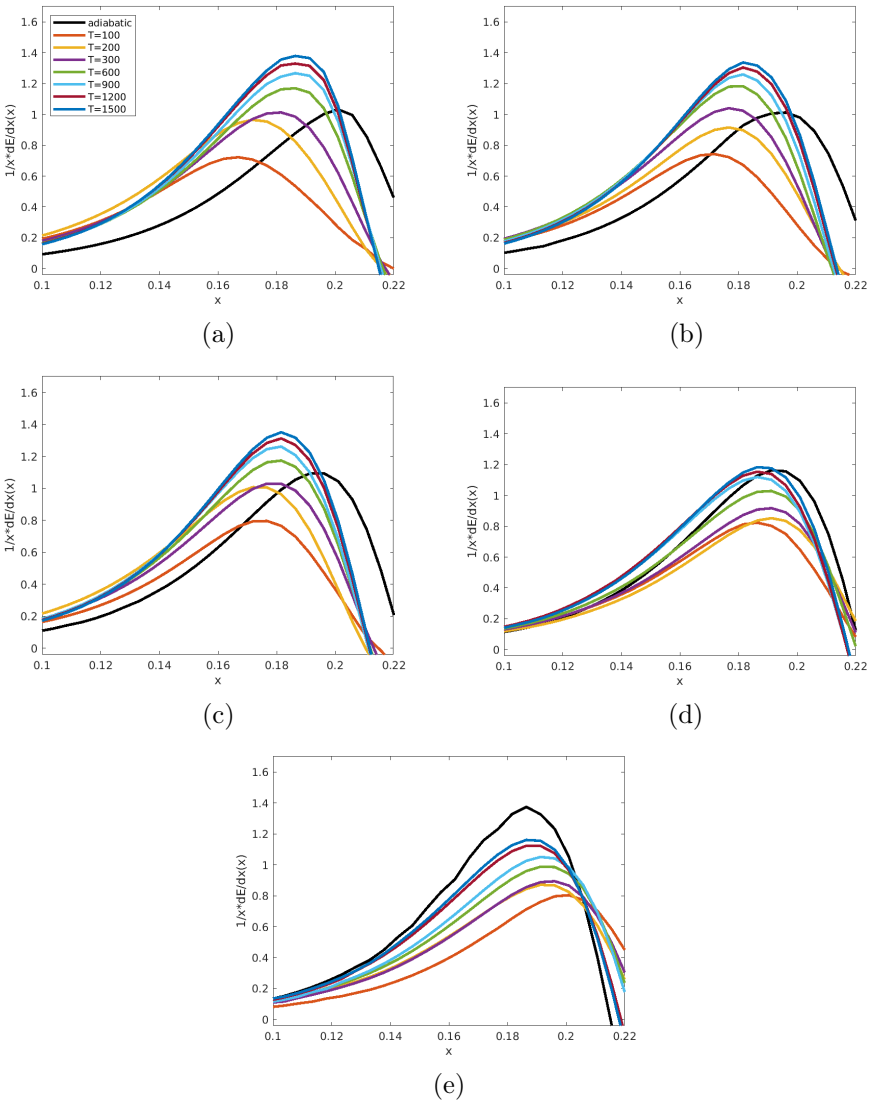

Figure 9. Energy growth profiles for wall-temperatures; 100 K, 200 K, 300 K, 600 K, 900 K, 1200 K, and 1500 K at different freestream Mach number conditions: a) $M = 2.0$**, b)** $M = 3.0$**, c)** $M = 4.0$**, d)** $M = 5.0$**, e)** $M = 6.0$

We calculate the spanwise averaged wall shear stress using the integral

$$\tau_w(x) = \frac{1}{(z_2 - z_1)} \int_{z_1}^{z_2} \left. \frac{\partial u}{\partial y} \right|_{y=0} (x, 0, z) dz \tag{23}$$

and plotted against x in figure 10. Here the trend is inverted: considering each Mach number case individually, the shear stress associated with the cooling and heating conditions is, respectively, higher and lower than that of the adiabatic case. However, as the streamwise Mach number is increased, the adiabatic flow temperature increases resulting in higher convection level at the wall, thus causing the shear stress to further decrease compared to the other isothermal cases. The shear stress gradually increases for all cases. The jump in the wall shear stress coincides (approximately) with the location at which the energy saturation initiates.

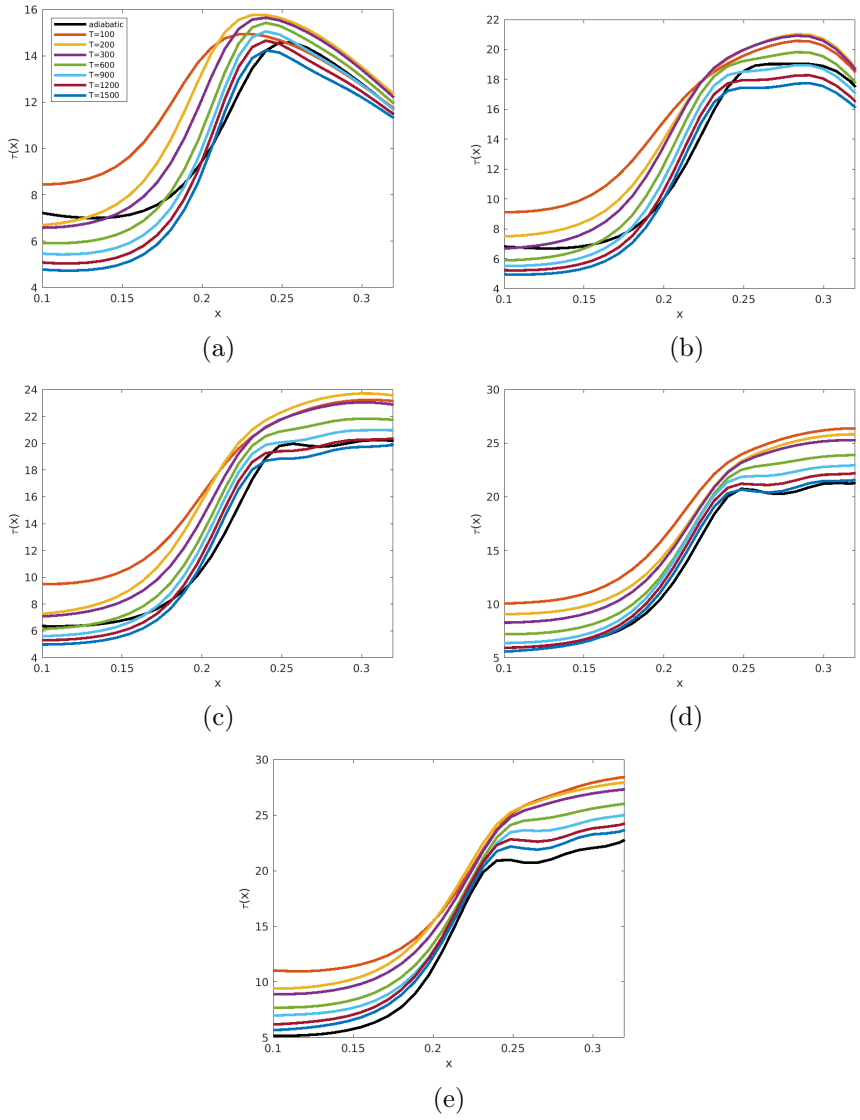

Figure 10. Spanwise averaged wall shear stress profiles for wall-temperatures; 100 K, 200 K, 300 K, 600 K, 900 K, 1200 K, and 1500 K at different freestream Mach number conditions: a) $M = 2.0$**, b)** $M = 3.0$**, c)** $M = 4.0$**, d)** $M = 5.0$**, e)** $M = 6.0$

We use equation 26 to calculate the spanwise averaged wall heat flux

$$q_w(x) = -\frac{1}{(z_2 - z_1)} \int_{z_1}^{z_2} \frac{\partial T}{\partial y}\bigg|_{y=0} (x, 0, z) dz, \tag{24}$$

we then plot it in figure 11 for the cooling and heating wall-conditions as a function of the streamwise coordinate (the null adiabatic heat flux is illustrated by the black dotted line). As expected, the cooling and heating cases respectively result in negative and positive heat flux values. The increase in the freestream Mach number result in a drop in the heat flux regardless of the wall-temperature condition, however, the reduction in the cooling cases is more significant.

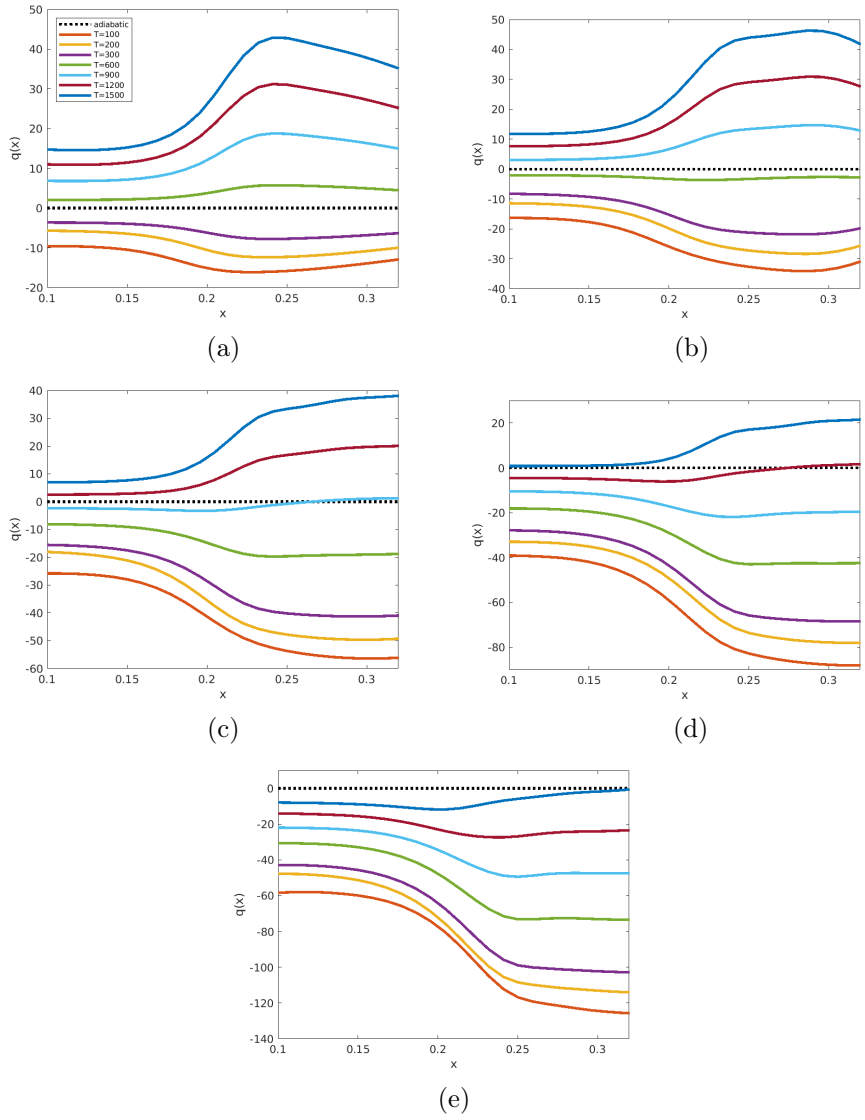

Figure 11. Spanwise averaged wall heat flux profiles for wall-temperatures; 100 K, 200 K, 300 K, 600 K, 900 K, 1200 K, and 1500 K at different freestream Mach number conditions: a) $M = 2.0$**, b)** $M = 3.0$**, c)** $M = 4.0$**, d)** $M = 5.0$**, e)** $M = 6.0$

IV. Conclusion

In this paper, we investigated streamwise/Görtler vortices developing in high-speed boundary layer flows using a numerical solution to the nonlinear compressible boundary region equations (NCBRE). We studied the nonlinear development of these secondary instabilities at different wall-temperature (including both heating and cooling) and freestream Mach number conditions . The disturbances in the boundary layer were excited using a small wall disturbance in the normal direction in the form of steady blowing and suction.

Contour plots of temperature at various crossflow planes showed the vortex development in the form of mushroom shape structures evolving in the streamwise direction. These vortices grow as the wall temperature is increased (heating) and shrink as the wall-temperature is decreased, still they appear to start growing again as the temperature at the wall is further decreased (i.e. at 100 K) suggesting closer examination. We observed that as the wall-temperature is increased with respect to the adiabatic wall condition, i.e. heating, the scaled kinetic energy an growth rate maximum increase as well while they decreased for the cooling wall-temperature cases. The same trend was also observed for the wall shear stress and the wall heat flux. The

jump of the wall shear stress appears to take place approximately at the streamwise location corresponding to the point of energy saturation initiation.

In the future, we intend to consider a wider range of wall-temperature conditions especially in the cooling case due to the peculiar pattern noticed in the temperature contour plots. We are also interested in combining parametric studies like the one presented in this paper with the optimal control formalism in an attempt to control the boundary layer in the compressible regime.

References

[1]Boiko, A.V., Ivanov, A.V., Kachanov, Y.S. and Mischenko, D.A. (2010) Steady and unsteady Görtler boundary-layer instability on concave wall, *European Journal of Mechanics B/Fluids*, Vol. 29, pp. 61-83.

[2]Choudhari, M. and Fischer, P. (2005) Roughness induced Transient Growth, *AIAA Paper 2005-4765.*

[3]Depmsey, L.D., Hall, P. & Deguchiu, K. (2017) The excitation of Gortler vortices by free stream coherent structures, *J. Fluid Mech.*, Vol. 826, pp. 60-96.

[4]Dryden, H. L. (1955) Transition from laminar to turbulent flow at subsonic and supersonic speeds. Conference on High-Speed Aeronautics, 41, Polytechnic of Brooklyn, New York.

[5]El-Hady N. M. & Verma, A. K. (1983) Growth of Görtler vortices in compressible boundary layers along curved surfaces. *J. Eng Appl. Sci.*, Vol. 2 (3), 213-238.

[6]Es-Sahli, O., Sescu, A., Afsar, M. and Hattori, Y. (2020) Investigation of Görtler vortices in high-sp eed b oundary layers via an efficient numerical solution to the non-linear boundary region equations. *TCFD.*

[7]Fedorov, A.V. (2015) Prediction and control of laminar-turbulent transition in high-speed boundary layers, Procedia IUTAM, Vol. 14, pp. 3-14.

[8]Goldstein, M., Sescu, A., Duck, P. and Choudhari, M. (2010) The Long Range Persistence of Wakes behind a Row of Roughness Elements, *Journal of Fluid Mechanics*, Vol. 644, pp. 123-163.

[9]Goldstein, M., Sescu, A., Duck, P. and Choudhari, M. (2011) Algebraic/transcendental Disturbance Growth behind a Row of Roughness Elements, *Journal of Fluid Mechanics*, Vol. 668, pp. 236-266.

[10]Goldstein, M., Sescu, A., Duck, P. and Choudhari, M. (2016) Nonlinear wakes behind a row of elongated roughness elements, *Journal of Fluid Mechanics*, Vol. 796, pp. 516-557.

[11]Goldstein, M. & Sescu (2008) Boundary-layer transition at high free-stream disturbance levels - beyond Klebanoff modes. *J. Fluid Mech.*, Vol. 613, pp. 95-124.

[12]Görtler, H . (1941) Instabilita-umt laminarer Grenzchichten an Konkaven Wanden gegenber gewissen dreidimensionalen Storungen, *ZAMM*, Vol. 21, pp. 250–52; english version: *NACA Report 1375* (1954)

[13]Gregory, N. and Walker, W.S. (1950) The effect on transition of isolated surface excrescences in the boundary-layer ıARC Technical Report 13, pp. 436; published as Aeronaut. Res. Council R&M 2779 (1956), pp. 1-10.

[14]Hall, P. (1982) Taylor-Görtler vortices in fully developed or boundary-layer flows: linear theory, *Journal of Fluid Mechanics*, Vol. 124, pp. 475-494.

[15]Hall, P. (1983) The linear development of Görtler vortices in growing boundary layers, *Journal of Fluid Mechanics*, Vol. 130, pp. 41-58.

[16]Hall, P. and Horseman. N. (1991) The linear inviscid secondary instability of longitudinal vortex structures in boundary layers. *Journal of Fluid Mechanics.* Vol. 232, pp. 357-375.

[17]Hall, P. & Fu, Y. 1989 On the Görtler vortex instability mechanism at hypersonic speeds. *Theor. Comput. Fluid Dyn.*, Vol. 1 (3), 125-134.

[18]Hall, P. & Malik, M. 1989 The growth of Görtler vortices in compressible boundary layers. *J. Engng Maths*, Vol. 23 (3), 239-251.

[19]Kendall, J. (1975) Wind tunnel experiments relating to supersonic and hypersonic boundary layer transition. *AIAA J.* 13, 290-299.

[20]Kendall, J.M. (1998) Experiments on boundary-layer receptivity to freestream turbulence. *AIAA Paper 2004-2335.*

[21]Kobayashi, R. & Kohama, Y. (1977) Taylor-Görtler instability of compressible boundary layers. *AIAA J.*, Vol. 15 (12), 1723-1727.

[22]Landahl, M.T. (1980) A note on an algebraic instability of inviscid parallel shear flows. *J. Fluid Mech.*, Vol. 98, pp. 243-251.

[23]Leib, S.J., Wundrow, W. & Goldstein, M. (1999) Effect of free-stream turbulence and other vortical disturbances on a laminar boundary layer. *J. Fluid Mech.*, Vol. 380, pp. 169-203.

[24]Li, F. and Malik, M. (1995) Fundamental and subharmonic secondary instabilities of Görtler vortices, *Journal of Fluid Mechanics*, Vol. 297, pp. 77-100.

[25]Li, F., Choudhari, M., Chang, C.-L., Greene, P., and Wu, M. (2010) Development and Breakdown of Gortler Vortices in High Speed Boundary Layers", 48th AIAA Aerospace Sciences Meeting Including the New Horizons Forum and Aerospace Exposition, Aerospace Sciences Meetings.

[26]Liu. X., Osher, S. and Chan, T. (1994) Weighted essentially non-oscillatory schemes, Journal of Computational Physics, Vol. 115, pp. 200-212.

[27]Mack, L. (1975) Linear stability theory and the problem of supersonic boundary layer transition. *AIAA J.* 3, 278-289.

[28]Malik, M.R. & Hussaini, M.Y. (1990) Numerical simulation of interactions between Gortler vortices and Tollmien-Schlichting waves. *J. Fluid Mech.*, Vol. 210, pp. 183-199.

[29]Marensi, E., Ricco, P. & Wu, X. (2017) Nonlinear unsteady streaks engendered by the interaction of free-stream vorticity with a compressible boundary layer. *J. Fluid Mech.*. Vol. 817, pp. 80-121.

[30]Matsubara, M. and Alfredsson, P.H. (2001) Disturbance growth in boundary layers subjected to free stream turbulence, *J. Fluid Mech.*, Vol. 430, pp. 149.

[31]Pate, S. R. (1971) Supersonic boundary-layer transition: effects of roughness and free-stream disturbances. *AIAA J.* 9, 797-803.

[32]Ren, J. & Fu, S. (2017) Secondary instabilities of Gortler vortices in high-speed boundary layer flows, *J. Fluid Mech.*, Vol. 781, pp. 388-421.

[33]Ricco, P. (2006) Response of a compressible laminar boundary layer to free-stream turbulence. PhD thesis, University of London.

[34]Ricco, P. & Wu, X. 2007 Response of a compressible laminar boundary layer to free-stream vortical disturbances, *J. Fluid Mech.*, Vol. 587, pp. 97-138.

[35]Ricco, P., Shah, D. & Hicks, P. D. (2013) Compressible laminar streaks with wall suction. *Phys. Fluids* 25, 054110.

[36]Ricco, P., Tran, D.-L. & Ye, G. (2009) Wall heat transfer effects on Klebanoff modes and Tollmien- Schlichting waves in a compressible boundary layer. *Phys. Fluids* 21, 024106.

[37]Saric, W.S. (1994) Görtler Vortices, *Annu. Rev. Fluid Mech.*, Vol. 26, pp. 379-409.

[38]Sescu, A., Taoudi, L. and Afsar, M. (2017) Iterative control of Görtler vortices via local wall deformations, *Theoretical and Computational Fluids Dynamics*, DOI 10.1007/s00162-017-0440-2.

[39]Sescu, A., Pendyala, R. and Thompson, D. (2014) On the Growth of Görtler Vortices Excited by Distributed Roughness Elements, AIAA Paper 2014-2885.

[40]Sescu, A. and Thompson, D. (2015) On the Excitation of Görtler Vortices by Distributed Roughness Elements, *Theoretical and Computational Fluids Dynamics*, Vol. 29, pp. 67-92.

[41]Schneider, S. P. (2001) Effect of high-speed tunnel noise on laminar-turbulent transition. *J. Sp. Rock.* 38-3, 323-333.

[42]Spall, R.E. and Malik, M.R. (1989) Görtler vortices in supersonic and hypersonic boundary layers, *Physics of Fluids A: Fluid Dynamics*, Vol. 1, pp. 1822.

[43]Swearingen, J.D. and Blackwelder, R.F. (1987) The growth and breakdown of streamwise vortices in the presence of a wall. *J. Fluid Mech.*, Vol. 182, pp. 255-290.

[44]Tam, C.K.W. and Webb, J.C. (1993), Dispersion-relation-preserving finite difference schemes for Computational Aeroacoustics, *Journal of Computational Physics*, Vol. 107, pp. 262-281.

[45]Tani, I. (1962) Production of longitudinal vortices in the boundary-layer along a curved wall, *J. Geophys. Res.*, Vol. 67, pp. 3075.

[46]Westin, K.J.A., Boiko, A.V., Klingmann, B.J.B., Kozlov, V.V. & Alfredsson, P.H. (1994) Experiments in a boundary layer subjected to free stream turbulence. part 1. Boundary layer structure and receptivity. *J. Fluid Mech.*, Vol. 281, pp. 193-218.

[47]White, E.B. (2002) Transient growth of stationary disturbances in a flat plate boundary layer, *Phys. Fluids*, Vol. 14, pp. 4429-4439.

[48]White, E.B., Rice, J.M. and Ergin, F.G. (2005) Receptivity of stationary transient disturbances to surface roughness, *Physics of Fluids*, Vol. 17, pp. 064109.

[49]Wu, X. and Choudhari, M. (2011) Linear and nonlinear instabilities of a blasius boundary layer perturbed by streamwise vortices. Part 2. Intermittent instability induced by long wavelength Klebanoff modes. *J. Fluid Mech.*. Vol. 483, pp. 249-286.

[50]Wu, X, Zhao, D. and Luo, J (2011) Excitation of steady and unsteady Görtler vortices by free-stream vortical disturbances, *Journal of Fluid Mechanics*, Vol. 682, pp. 66-100.

[51]Xu, D., Zhang, Y. & Wu, X. (2017) Nonlinear evolution and secondary instability of steady and unsteady Gortler vortices induced by free-stream vortical disturbances, *J. Fluid Mech.*, Vol. 829, pp. 681-730.

[52]Xu, G., Xiao, Z. & Fu, S. (2011) Secondary instability control of compressible flow by suction for a swept wing, Physics, Mechanics & Astronomy, Vol. 54, pp. 2040-2052.

[53]Zaki, T.A. & Durbin, P. (2005) Mode interaction and the bypass route to transition. *J. Fluid Mech.*, Vol. 531, pp. 85-111.